ARTICLE

Effect of Chemical Modification of Fullerene-Based Self-Assembled Monolayers on the Performance of Inverted Polymer Solar Cells

Steven K. Hau,[†] You-Jung Cheng,[†] Hin-Lap Yip,[†,‡] Yong Zhang,[†] Hong Ma,[†] and Alex K.-Y. Jen*[,†,‡]

Department of Materials Science and Engineering and Institute of Advanced Materials and Technology, University of Washington, Seattle, Washington 98195

ABSTRACT The interface of electron-selective ZnO in inverted polymer bulk-heterojunction (BHJ) solar cells was modified with a series of fullerene-based self-assembled monolayers (C_{60}-SAM) containing different anchoring groups (catechol, carboxylic acid, and phosphonic acid), linkage location, and functionalization. The formation of the C_{60}-SAM to the surface of ZnO was investigated by processing the SAM through either a solution immersion technique or a solution spin-coating method. It is found that the C_{60}-SAMs with the carboxylic acid and catechol termination can be formed onto the surface of ZnO by simple solution spin-coating process, whereas all three anchoring groups can be formed by solution immersion technique. Heterojunction devices were fabricated under different processing conditions to form SAM leading to 2-fold, 75%, and 30% efficiency improvement with the carboxylic acid, catechol, and phosphonic acid C_{60}-SAMs, respectively. The main contribution to the variation of efficiency from different SAMs is due to the open circuit voltage affected by different anchoring groups and functionalization of the C_{60}-SAM. The results from BHJ devices show an efficiency enhancement of ~6−28% compared to devices without SAM modification because of the improved photoinduced charge transfer from polymer to the C_{60}-SAM/ZnO. The SAM formation condition influences the device performance. Because of the strong acidic nature of the phosphonic acid anchoring group, immersing the ZnO substrate into a solution containing the C_{60}-phosphonic acid SAM for an extended period of time will lead to degradation of the ZnO surface. This in turn, leads to devices without any photovoltaic activity, whereas weaker acids like carboxylic acid and catechol-based C_{60}-SAMs can be assembled onto ZnO, leading to devices with average efficiencies of 4.4 and 4.2%, respectively.

KEYWORDS: fullerene • self-assembled monolayer • inverted polymer solar cells

INTRODUCTION

Solution-processable polymer-based solar cells (PSCs) can be a low-cost option for renewable energy because of their potential for fabricating large-area flexible modules. On the basis of the bulk-heterojunction (BHJ) concept using blends of p-type semiconducting polymers and n-type semiconducting fullerenes, efficiencies greater than 6% have been attained (1−3). The two main types of device architectures that have been used to fabricate PSCs are the conventional and inverted structures. The conventional structure is the most widely used architecture to fabricate PSCs. In this architecture, a transparent conducting indium tin oxide (ITO) is utilized as the anode to collect holes and a low work function metal is used as the cathode to collect electrons. Typically, a thin conducting hole transporting layer of poly(3,4-ethylenedioxythiophene):poly(styrenesulfonate) (PEDOT:PSS) is deposited onto ITO to help planarize the rough ITO surface as well as to increase its work function to facilitate better hole collection. However, PEDOT:PSS has been shown to cause instability at the ITO interface due to its acidic nature leading to etching of the metal oxide (4). Additionally, the low work function metal in this architecture can be easily oxidized in air leading to degradation of the devices (5).

To alleviate this problem, the inverted device structure where the nature of charge collection is reversed was proposed as a good alternative architecture. In this architecture, modification of the bottom ITO electrode with a suitable electron-transporting/hole-blocking buffer layer for electron collection is utilized while a hole-transporting/electron-blocking buffer to facilitate efficient hole collection is utilized at the top between the bulk-heterojunction layer and high work-function metal electrode. The higher work function metals utilized in this architecture have the advantage of improving air-stability, which prolongs the lifetime of the device in ambient (5). In addition, with an appropriate buffer layer applied on top of the bulk-heterojunction active layer, silver metal nanoparticles can be printed and coated from solution onto these inverted cells to replace high vacuum deposited electrodes (6).

Among the few available electron-transporting/hole-blocking buffer layers that have been used for inverted

* Corresponding author. E-mail: ajen@u.washington.edu.
Received for review March 18, 2010 and accepted June 3, 2010
[†] Department of Materials Science and Engineering, University of Washington.
[‡] Institute of Advanced Materials and Technology, University of Washington.
DOI: 10.1021/am100238e

Published on Web 06/15/2010

polymer-based solar cells, ZnO has been of interest recently due to its high electron mobility as well as the ease to generate various shape and size nanostructures for inorganic/organic hybrid solar cells (7, 8). However, hydroxyl terminated metal oxides are known to act as electron charge traps, which can affect the electrical properties at the interface between the metal oxide and organic layers (9). Improving the electrical coherence between these materials is important especially in polymer-based solar cells as recombination losses at these interfaces can drastically affect the potential for photocurrent collection. Interface modifiers with self-assembling properties have been used to improve the charge transfer between organic layers and metal oxides through covalently bonding the modifiers onto the surface of the metal oxide. The modifier can serve multiple purposes, including to help passivate surface charge traps to improve forward charge transfer, tune the energy level offset between semiconductors and organic layers, and affect the upper organic layer morphology (10−12). Common modifiers on metal oxides have been based on phosphonic acid and carboxylic-acid-terminated anchoring groups because of their strong affinity to various metal oxide surfaces (13−18). Carboxylic acid terminated modifiers have been generally employed onto TiO_2-based systems for use in photovoltaics (19). However, the application of carboxylic acid terminated and phosphonic acid terminated modifiers onto the surface of ZnO have shown to potentially degrade and etch the ZnO layer because of the acidic nature of the molecules (20). To reduce the potential etching of ZnO, we should utilize modifiers with less-acidic binding terminal units. Use of catechol termination for modifiers is quite attractive because of its weak diprotic acid nature and its ability to form bidentate bonding with metal oxides (21, 22).

Previously, C_{60}-based self-assembled monolayer (SAM) modifiers with carboxylic acid anchoring group were formed on the ZnO nanoparticle electron selective layer of polymer BHJ inverted solar cells showing an improved device efficiency (23). It is found that the morphology of the active layer and the charge transfer at the interface between the metal oxide and active layer is better with the C_{60}-SAM modification. Because the quality of this interface is important in attaining high-performance devices, electron-selective layers of ZnO nanoparticles functionalized with C_{60}-based SAMs using three different anchoring groups (carboxylic-acid-terminated, catechol-terminated, and phosphonic-acid-terminated) are systematically investigated to observe the effect of the binding group on the performance of inverted solar cells. In addition to the three C_{60}-SAMs with different anchoring groups, the influence of two additional SAMs on inverted solar cell performance are investigated by changing the linkage geometry of the carboxylic acid anchoring group to C_{60} and functionalizing a carboxylic acid anchoring group onto PCBM.

The effect of the binding group, linkage, and bis-functionalization of C_{60} on the charge transfer properties from the C_{60}-SAM layer at the interface between ZnO-NPs and P3HT is studied with heterojunction solar cells. The open-circuit voltage and fill factor changes are dependent on the SAM at the interface. However, these differences are less evident in bulk-heterojunction devices, because of the main controlling parameter is primarily from the interface between the donor and acceptor blends. Since the affinity of the anchoring groups to the surface of ZnO are different, the C_{60}-SAMs are processed and formed onto the layer of ZnO nanoparticles by either a solution immersion technique or by a solution spin-coating method.

It is found that the C_{60}-SAMs with either the carboxylic acid or catechol end-group can be formed onto the surface of ZnO by a simple solution spin-coating process, whereas all three anchoring groups can be formed onto ZnO by a solution immersion technique. The optimum time for solution immersion is dependent on the anchoring group due to their differences in binding affinity to ZnO. The different processing method of the C_{60}-SAM on ZnO, the anchoring group, the linkage, and the functionalization on the C_{60}-SAM leads to improved performance (as high as 28%) of inverted BHJ solar cells compared to devices without SAM modification. However, due to the strong acidic nature of the phosphonic acid anchoring group, immersing the ZnO substrate into a solution containing the C_{60}-phosphonic acid SAM for a long period of time can cause degradation and etching of the ZnO surface leading to poor solar cell efficiencies, whereas weaker acids like carboxylic acid and catechol-based C_{60}-SAMs can be assembled onto ZnO, leading to higher efficiency solar cells.

EXPERIMENTAL SECTION

Materials. Regioregular poly(3-hexyl-thiophene) (P3HT, 4002-E grade) was purchased from Rieke Metals, Inc. and was used as received without further purification. The [6,6]-phenyl C_{61} butyric acid methyl ester (PCBM) was purchased from American Dye Source Inc. (99.0% purity), and was used as received without further purification. All chemicals were purchased from Aldrich and used as-received unless otherwise specified. Triethylamine was distilled over CaH_2, and toluene and methylene chloride were distilled over P_2O_5. ^{1}H NMR spectra (300 MHz) were taken on a Bruker-300 FT NMR spectrometer with tetramethylsilane (TMS) as internal reference. Elemental analysis was determined at QTI (Whitehouse, NJ). ESI-MS spectra were obtained on a Bruker Daltonics Esquire ion trap mass spectrometer. The thermal properties (see the Supporting Information, Figure S2) of the fullerene-based SAMs were measured by differential scanning calorimetry (DSC) using the DSC2010 (TA Instruments) under a heating rate of 10 °C min^{-1} and a nitrogen flow of 50 mL min^{-1}.

Synthesis of the five different C_{60}-SAM molecules is shown in Scheme 1.

Synthesis of C_{60}-Substituted Benzoic Acid (SAM[1]). A mixture of 4-carboxybenzaldehyde (0.210 g, 1.40 mmol), C_{60} (0.202 g, 0.28 mmol), and *N*-methylglycine (0.125 g, 1.40 mmol) in chlorobenzene (60 mL) was refluxed overnight under a nitrogen atmosphere. The solvent was removed by rotary evaporation under reduced pressure. The crude product was purified over silica gel column chromatography with toluene to toluene/THF (2/1) as the eluents to afford a brown-yellow solid (0.238 g, 95%). ^{1}H NMR (300 MHz, DMSO-d$_6$): δ 2.20 (s, 3H), 6.65 (s, 1H), 6.89 (s, 2H), 8.03 (d, J = 8.4 Hz, 2H), 8.15 (d, J = 8.4 Hz, 2H), 10.12 (s, 1H). Calcd for $C_{70}H_{11}NO_2$: C, 93.64; H, 1.23; N, 1.56. Found: C, 93.45; H, 1.31; N, 1.62. ESI-MS (*m*/*z*): calcd, 897.1; found, 897.0.

Scheme 1. Synthesis of C_{60}-Substituted Benzoic Acid, Catechol, Phenylphosphonic Acid, Benzoic Acid with Different Linkage, and PCBM-Substituted Benzoic Acid

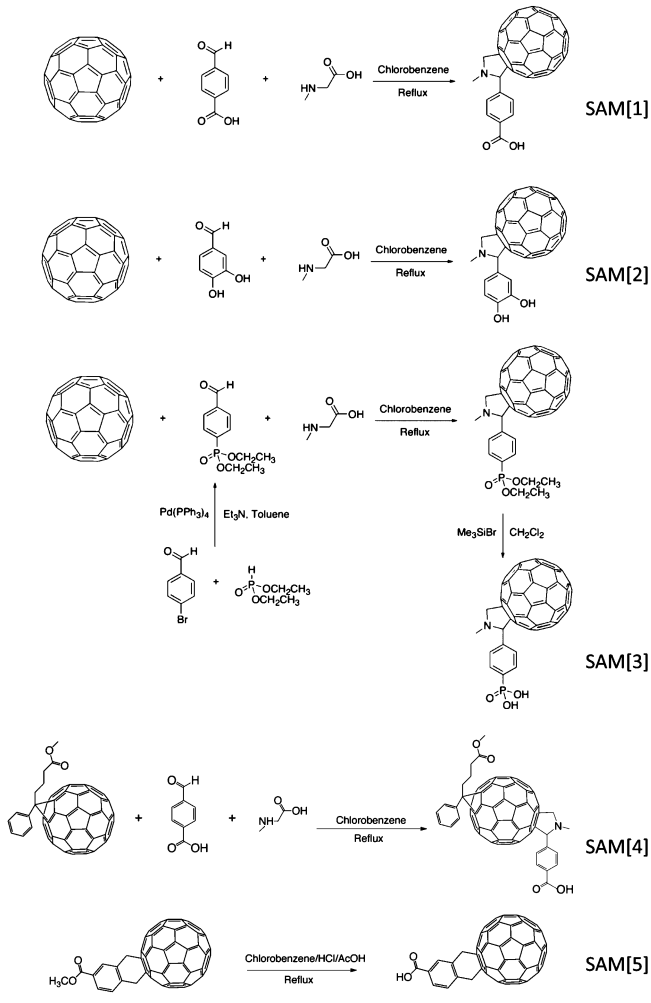

Synthesis of C_{60}-Substituted Catechol (SAM[2]). A mixture of 3,4-dihydroxybenzaldehyde (0.193 g, 1.40 mmol), C_{60} (0.202 g, 0.28 mmol), and *N*-methylglycine (0.125 g, 1.40 mmol) in chlorobenzene (60 mL) was refluxed overnight under a nitrogen atmosphere. The solvent was removed by rotary evaporation under reduced pressure. The crude product was purified over silica gel column chromatography with toluene to toluene/THF (2/1) as the eluents to afford a brown solid (0.181 g, 73%). ^{1}H NMR (300 MHz, DMSO-d_6): δ 2.15 (s, 3H), 5.20 (s, 2H), 6.38 (d, J = 4.5 Hz, 1H), 6.46 (d, J = 8.4 Hz, 1H), 6.48 (dd, J = 4.5 8.4 Hz, 1H), 6.57 (s, 1H), 6.78 (s, 2H). Calcd for $C_{69}H_{11}NO_2$: C, 93.55; H, 1.25; N, 1.58. Found: C, 93.47; H, 1.30; N, 1.64. ESI-MS (*m*/*z*): calcd, 885.1; found, 885.0.

Synthesis of Diethyl 4-Aldehydephenylphosphonate. A mixture of 4-bromobenzaldehyde (2.78 g, 15.0 mmol), diethyl phosphite (2.49 g, 18.0 mmol), and $Pd(PPh_3)_4$ (0.867 g, 0.75 mmol) in dry toluene (20 mL) and dry triethylamine (20 mL) was stirred and heated at 80 °C overnight under a nitrogen atmosphere. The solvent was removed by rotary evaporation under reduced pressure. The crude product was extracted with methylene chloride three times, washed with water two times, dried over Na_2SO_4, and purified over silica gel column chromatography with methylene chloride to methylene chloride/ethyl acetate (1/1) as the eluents to afford a yellow solid (2.33 g, 64%). ^{1}H NMR (300 MHz, $CDCl_3$): δ 1.10 (t, J = 3.6 Hz, 6H), 3.56 (q, J = 3.6 Hz, 4H), 7.90 (d, J = 8.1 Hz, 2H), 7.94 (d, J = 8.1 Hz, 2H), 9.86 (s, 1H). Calcd for $C_{11}H_{15}O_4P$: C, 54.55; H, 6.24; P, 12.79. Found: C, 54.45; H, 6.20; P, 12.87. ESI-MS (*m*/*z*): calcd, 242.1; found, 242.1.

Synthesis of Diethyl (C_{60}-Substituted)phenylphosphonate. A mixture of diethyl 4-aldehydephenylphosphonate (0.424 g, 1.75 mmol), C_{60} (0.252 g, 0.35 mmol), and *N*-methylglycine (0.156 g, 1.75 mmol) in chlorobenzene (75 mL) was refluxed overnight under a nitrogen atmosphere. The solvent was removed by rotary evaporation under reduced pressure. The crude product was purified over silica gel column chromatography with toluene to toluene/THF (1/1) as the eluents to afford a brown solid (0.273 g, 79%). ^{1}H NMR (300 MHz, DMSO-d_6): δ 1.11 (t, J = 3.6 Hz, 6H), 2.15 (s, 3H), 3.57 (q, J = 3.6 Hz, 4H), 6.65 (s, 1H), 6.89 (s, 2H), 7.25 (d, J = 8.1 Hz, 2H), 7.65 (d, J = 8.1 Hz, 2H). Calcd for $C_{73}H_{20}NO_3P$: C, 88.57; H, 2.04; N, 1.41; P, 3.13. Found: C, 88.45; H, 1.95; N, 1.52; P, 3.19. ESI-MS (*m*/*z*): calcd, 989.1; found, 989.1.

Synthesis of C_{60}-Substituted Phenylphosphonic Acid (SAM[3]). To a solution of diethyl (C_{60}-substituted)phenylphosphonate (0.273 g, 0.276 mmol) in dry methylene chloride (20 mL) under a nitrogen atmosphere was added bromotrimethylsilane (0.63 mL, 0.750 g, 4.9 mmol). The reaction mixture was stirred overnight at room temperature, poured into water (200 mL), filtered and washed with water (200 mL). The product was collected and dried to afford a brown solid (0.201 g, 78%). δ 2.15 (s, 3H), 6.63 (s, 1H), 6.81 (s, 2H), 7.23 (d, J = 8.1 Hz, 2H), 7.60 (d, J = 8.1 Hz, 2H). Calcd for $C_{69}H_{12}NO_3P$: C, 88.75; H, 1.30; N, 1.50; P, 3.32. Found: C, 88.83; H, 1.33; N, 1.42; P, 3.24. ESI-MS (*m*/*z*): calcd, 933.1; found, 933.0.

Synthesis of PCBM-Substituted Benzoic Acid (SAM[4]). The PCBM-substituted benzoic acid was synthesized using the similar procedure of C_{60}-substituted benzoic acid. The resulted bis-functionalized PCBM-substituted benzoic acid is the mixture of isomers. ^{1}H NMR (300 MHz, $CDCl_3$): 10.15 (s, 1H), 8.30 (d, J = 8.2 Hz, 2H), 8.20−7.90 (m, 2H), 8.03 (d, J = 8.4 Hz, 2H), 7.90−7.30 (m, 3H), 7.00 (s, 2H), 6.58 (s, 1H), 3.78−3.56 (m, 3H), 2.86−2.72 (m, 2H), 2.61−2.37 (m, 2H), 1.90−1.86 (m, 2H). $C_{82}H_{25}NO_4$: Calcd: C, 90.52; H, 2.32; N, 1.29. Found: C, 90.68; H, 2.37; N, 1.27. ESI-MS (*m*/*z*): calcd, 1087.2; found, 1086.0.

Synthesis of C_{60}-Substituted Benzoic Acid (SAM[5]). To a solution of methyl (C60-substituted) benzoate (100 mg, 0.115 mmol) in chlorobenzene (50 mL) was added concentrated aqueous HCl (10 mL) and acetic acid (20 mL) under a nitrogen atmosphere. The reaction mixture was refluxed overnight. After cooling to room temperature, the solvent was removed under vacuum. The product was collected to afford a brown-dark solid. ^{1}H NMR (300 MHz, DMSO-d_6): 8.34 (s, 1H), 8.15 (d, J = 7.7 Hz, 2H), 7.91 (d, J = 8.0 Hz, 2H), 5.06 (m, 2H), 4.66 (m, 2H). Calcd for $C_{69}H_8O_2$: C, 95.39; H, 0.93. Found: C, 95.41; H, 0.96. ESI-MS (*m*/*z*): calcd, 868.1; found, 868.2.

Device Fabrication. To fabricate the ITO electrode based inverted solar cells, ITO-coated glass substrates (15 Ω/□) were cleaned with detergent, deionized water, acetone, and isopropyl alcohol for 10 min each step. The substrates were dried under a nitrogen stream. A thin layer of ZnO nanoparticles (ZnO-NPs) (~50 nm), synthesized using the method described by Beek et al. was spin-coated onto the ITO-coated glass (24). To form the monolayer of the C_{60}-SAM onto the ZnO-NPs by the spin-coating method: First, a 1 mM solution containing the SAM in a 1:1 (v:v) cosolvent of either tetrahydrofuran:chlorobenzene (THF:CB) or pure dimethylsulfoxide (DMSO) is prepared depending on the C_{60}-SAM anchoring group. For the carboxylic-acid- and catechol-terminated C_{60}-SAMs, a THF:CB solution is prepared, whereas for the phosphonic-acid-terminated C_{60}-SAM, a pure DMSO solution is prepared. The solutions are filtered through 0.2 μm PTFE filter prior to using the solutions for spin-coating. Solutions are cast onto the ZnO substrate and spun at 3500 rpm

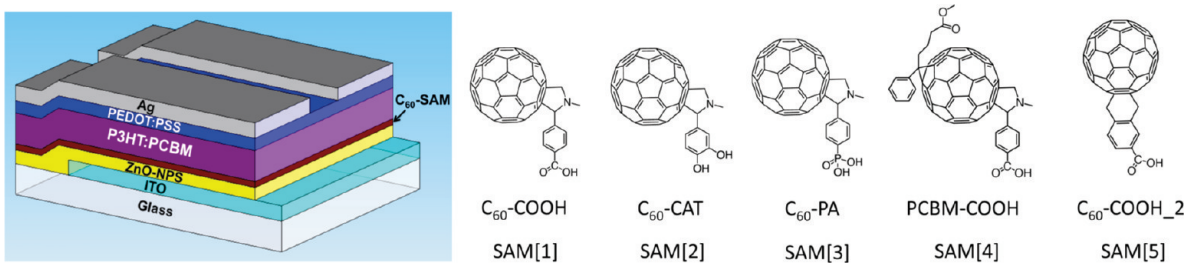

FIGURE 1. Device architecture of the inverted solar cell using different C_{60}-SAMs. (left to right) The five C_{60}-based molecules containing different anchoring groups and functionalization used for self-assembly on ZnO-NPs: C_{60}-COOH SAM[1], C_{60}-CAT SAM[2], C_{60}-PA SAM[3], PCBM-COOH SAM[4], and C_{60}-COOH_2 SAM[5].

for 1 min, after which any excess unbound SAMs are rinsed away with either THF:CB or DMSO.

To form the monolayer of the C_{60}-SAM onto the ZnO-NPs by the solution immersion technique: First, a 0.05 mM concentration solution of the C_{60}-SAMs are prepared in either THF:CB or DMSO depending on the anchoring group. The solutions are filtered through a 0.2 μm PTFE filter prior to immersion of the samples into the solution. The ZnO substrates are immersed into a 5 mL solution of the C_{60}-SAMs and left in solution for a set period of time (from 1 min up to 240 min). The samples are then removed from the solution and thoroughly rinsed with THF:CB or DMSO to remove any excess unbound molecules and dried under a nitrogen stream. The samples are transferred into an argon-filled glovebox for spin-coating of the active layer. A chlorobenzene solution containing poly(3-hexylthiophene) (P3HT) (Rieke Metals, 4002-E) and [6,6]-phenyl C_{61}-butyric acid methyl ester (PCBM) (American Dye Source) (60 mg/mL) with a weight ratio of (1:0.7) was spin-coated on the ZnO modified layer to achieve a thickness of (~210 nm) and annealed at 160 °C for 10 min for the bulk-heterojunction samples, whereas a 15 mg/mL concentration of P3HT in chlorobenzene was used to spin-coat heterojunction devices (~60 nm) and annealed at 160 °C for 10 min. After annealing, PEDOT:PSS (CLEVIOS P VP Al 4083) was spin-coated onto the active layer to achieve a thickness of ~50 nm and annealed for 10 min at 120 °C as previously described (11). The silver electrode was vacuum deposited (100 nm) at a pressure of 1×10^{-6} Torr to complete the device architecture.

Device Characterization. The unencapsulated solar cells were tested under ambient conditions using a Keithley 2400 SMU and an Oriel Xenon lamp (450 W) with an AM1.5 filter. A mask was used to define the device illumination area of 0.0314 cm^2 which is similar in size to the device electrode to minimize photocurrent generation from the edge of the electrodes (25, 26). The light intensity was calibrated to 100 mW/cm^2 using a calibrated silicon solar cell with a KG5 filter that has been previously standardized at the National Renewable Energy Laboratory.

The surface quality of the ZnO-NP layer before and after the C_{60}-SAM modification was characterized by imaging with an atomic force microscope (AFM) and scanning electron microscope (SEM). The AFM images were acquired under tapping mode using a Veeco multimode AFM with a nanoscope III controller. The SEM images were acquired using a FEI Sirion SEM at an accelerating voltage of 5 kV, a spot size of 3, working distance of 5 mm, and magnification of 50 000×. The surface energies for the C_{60}-SAM modified and unmodified ZnO-NPs substrates were calculated from measuring the advancing contact angle using deionized water and diiodomethane as probing solvents on a Ramé-Hart 100 Goniometer.

RESULTS AND DISCUSSION

A series of C_{60}-based SAM molecules are developed for improving the interfaces between the ZnO electron selective layer and active layer of inverted polymer solar cells. The influence of the different anchoring groups (carboxylic acid, catechol, phosphonic acid) using the same linkage to the C_{60} molecule on the binding to the ZnO-NPs layer and their affects on the device performance is evaluated. To further elucidate the affect and role of the C_{60}-SAM at the interface, we used a set of SAMs using the carboxylic-acid-terminated group as the binding component to the surface of ZnO while altering the linkage and functionalization to the C_{60} molecule. The syntheses of a series of C_{60}-based SAM molecules are shown in Scheme 1. C_{60}-based molecules with binding groups of carboxylic acid (C_{60}-COOH) and catechol (C_{60}-CAT) were obtained by [2 + 3] cycloadditions of C_{60} and the corresponding azomethine ylides formed from the reactions of *N*-methylglycine with 4-aldehydebenzoic acid and 3,4-dihydroxybenzaldehyde, respectively. C_{60}-based molecule with phosphonic acid binding group (C_{60}-PA) was prepared by [2 + 3] cycloaddition of C_{60} and the azomethine ylide formed from the reaction of *N*-methylglycine with diethyl 4-aldehydephenylphosphonate followed by the conversion of the diethyl C_{60}-phenylphosphonate to ditrimethylsilyl C_{60}-phenylphosphonate with bromotrimethylsilane and further hydrolysis with water. C_{60}-COOH_2 was obtained by the hydrolysis of its methyl C_{60}-benzoate precursor with a mixture of hydrochloric acid and acetic acid in chlorobenzene as followed by a previous literature method (27). PCBM-COOH was synthesized by [2 + 3] cycloaddition with the starting materials of PCBM, 4-aldehydebenzoic acid and *N*-methylglycine refluxed in chlorobenzene. The series of five C_{60}-based SAMs (C_{60}-COOH, C_{60}-CAT, C_{60}-PA, PCBM-COOH, and C_{60}-COOH_2) containing different anchoring groups, linkage, and functionalization are shown in Figure 1. For simplicity, the C_{60}-SAMs will from now on be referred to as SAM[1], SAM[2], SAM[3], SAM[4], and SAM[5] as labeled in Figure 1.

C_{60} Self-Assembled Monolayer (SAM) Formation on ZnO. The formation of the C_{60}-SAM layer onto the surface of the electron selective ZnO-NPs is dependent on the binding affinity of the anchoring group to the surface of the ZnO. To assess to binding ability of the different C_{60}-SAM anchoring groups, we made solutions of each SAM as described in the Experimental Section; the layer of C_{60}-SAM is formed either by spin-coating from a concentrated solution or by immersing the substrates into solution for a set time. Contact angle and surface energy measurements are

used as a method to characterize the ZnO surface with and without the SAM modification to probe the formation of C_{60}-SAM layer on the surface. Prior to formation of the SAM onto the surface of the ZnO-NPs, the contact angle of the surface to deionized water is 30.5° and the surface energy was calculated to be 65.5 dyn/cm.

The formation of the C_{60}-SAM onto ZnO is first evaluated using a simple solution spincoating method of the concentrated (1 mM) SAM solution onto the layer of ZnO-NPs. Solvents are then used to rinse away any unbound molecules from the surface and dried prior to measuring contact angles. Processing the series of SAMs by spin-coating shows increased contact angles of 67.8, 54.2, 47.8, 55.1, and 73.3° for SAM[1], SAM[2], SAM[3], SAM[4], and SAM[5], respectively, compared to the unmodified layer of ZnO-NPs, indicating that the molecules are binding to the surface. However, the contact angles for SAM[2] and SAM[3] are low, indicating that the affinity of the SAM with catechol termination and phosphonic acid termination to the layer of ZnO-NPs using the spin-coating process is not as good compared to SAM[1] and SAM[5], which have a carboxylic acid termination. The contact angle for SAM[4] is also relatively low even though it contains a carboxylic acid anchoring group. The reason for the lower contact angle is due to the phenyl butyric acid methyl ester unit on the C_{60} that influences the surface energy.

The reactivity of some of the SAM binding groups may not be high enough to fully react with the surface due to the limited time exposure (<30 s) of the molecules to the ZnO-NPs surface during the spin-coating process. Therefore, to optimize the self-assembly process, a time-dependent immersion study by placing the substrates in solution for set time intervals will give a better indication of reactivity and affinity of the different C_{60}-SAM anchoring groups to the ZnO surface. Substrates were placed into dilute solutions (0.1 mM) of the C_{60}-SAMs at set time intervals ranging from 1 to 240 min and are removed and rinsed with solvents to remove any unbound molecules. Contact angles are measured for each time interval to attain the optimum self-assembly time of each SAM (see the Supporting Information, Figure S2).

For SAM[1] containing the carboxylic acid anchoring group, the optimum solution self-assembly time is around 10−30 min, giving contacts angles in the low 70s and calculated surface energies in the low 50s. These values are similar to that of spin-coating SAM[1] from a higher concentration solution, indicating that the simple spin-coating method can form a good SAM onto the ZnO-NP surface. However, longer assembly time shows a decrease in contact angle and an increase in surface energy signifying that the surface may be changed.

For SAM[4] and SAM[5] which also contain carboxylic acid based anchoring groups show an optimum assembly time of 10−30 min. Assembly of the SAMs for longer time does not show any significant changes in the contact angles and surface energies. The C_{60}-SAM with the phenyl butyric acid methyl ester unit (SAM[4]) has an optimized contact angle in the low 60s while SAM[5] has a similar contact angle to SAM[1]. The optimized contact angles for SAM[5] by solution immersion assembly is similar to those processed by high concentration spin-coating whereas the processed contact angle values for SAM[4] are lower than those optimized using the solution immersion method. The lower contact angles of SAM[4] by spin-coating suggests that the affinity of the SAM to the ZnO surface is not as good as SAM[1] and SAM[5]. The catechol (SAM[2]) and phosphonic acid (SAM[3]) anchoring SAM show optimum assembly times around 10 min with contact angles in the high 50s to low 60s. The catechol based SAM has a slightly lower contact angle when spin-coated compared to the optimized solution immersion method suggesting that the reactivity of catechol to the ZnO surface is not as fast compared to the carboxylic acid. The phosphonic-acid-based SAMs have low contact angles when spin-coated and are optimized under solution assembly for 10 min, but assembly over 10 min shows a significant decrease in contact angle, signifying that the surface might be altered.

Surface Characterization of the C_{60}-SAM on ZnO. To identify what may be causing these changes in contact angles, the surface of the ZnO-NPs are characterized using both atomic force microscopy (AFM) and scanning electron microscopy (SEM). Figure 2 shows the AFM images of the ZnO-NPs without any surface modification and those modified with different C_{60}-based SAMs at the optimized solution immersion assembly time of 10 min and ones that are assembled for a longer time of 240 min. The substrate without any modification of the ZnO-NPs has a surface roughness of 3.65 nm rms. After modification of the ZnO-NPs surface with the C_{60}-SAMs under the optimized solution immersion assembly time of 10 min, there is no apparent change in the surface topography and the surface roughness of the samples are similar to those without modification. Assembly times of 240 min also show similar surface topography and surface roughness for all the C_{60}-SAMs except for SAM[3] which has a phosphonic acid anchoring group. At this assembly time, the surface roughness of SAM[3] on ZnO-NPs shows a drastic increase in roughness to 4.66 nm rms. This change in the roughness is attributed to the strong acidic nature of the phosphonic acid anchoring group that etches and damages the surface of the ZnO.

To further confirm the etching and damaging of the ZnO-NPs from the longer exposure of the acidic phosphonic acid SAM to the ZnO, the surface was further characterized using SEM. Figure 3 shows the images acquired from SEM on an unmodified ZnO-NPs surface compared to the five different C_{60}-SAMs that were assembled for 240 min using the solution immersion technique. The SEM image shows that the unmodified ZnO-NPs are relatively smooth and dense. From the images, a clear contrast can be observed between the unmodified ZnO-NPs surface to that of the one modified with the phosphonic acid C_{60}-SAM. The surface of the phosphonic acid C_{60}-SAM modified ZnO-NPs shows significant etching into the ZnO-NPs layer as seen by the large number of voids in the SEM image. This void formation at longer assembly

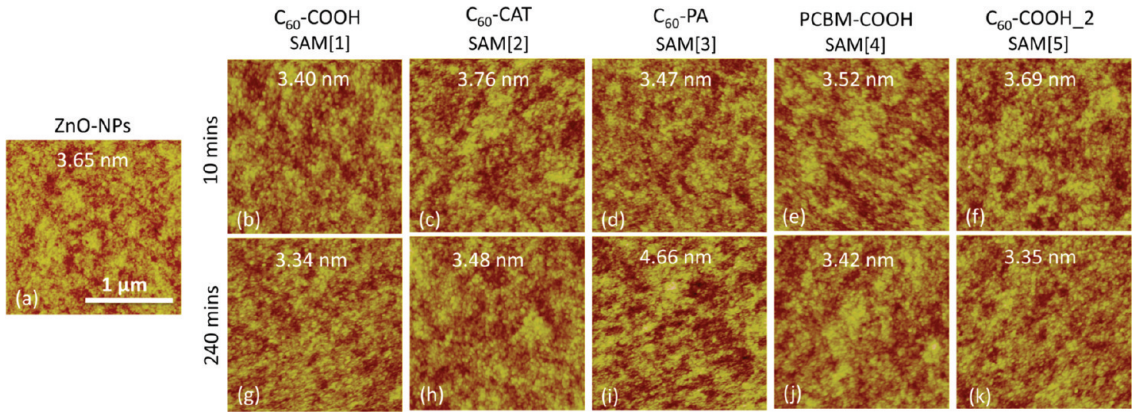

FIGURE 2. AFM image of (a) Bare ZnO-NPs on ITO, 10 min assembly of (b) C_{60}-COOH SAM, (c) C_{60}-CAT SAM, (d) C_{60}-PA SAM, (e) PCBM-COOH SAM, (f) C_{60}-COOH_2 SAM on ZnO-NPs, and 240 min assembly of (g) C_{60}-COOH SAM, (h) C_{60}-CAT SAM, (i) C_{60}-PA SAM, (j) PCBM-COOH SAM, (k) C_{60}-COOH_2 SAM on ZnO-NPs. The values inserted on the images are the rms roughness values of the ZnO-NP surface. All roughness values of the modified and unmodified surfaces are similar except for the C_{60}-PA SAM that is assembled for 240 min, which shows higher surface roughness, indicating degradation and etching of the ZnO surface. All scans are 2 μm × 2 μm and are on the same height scale (40 nm).

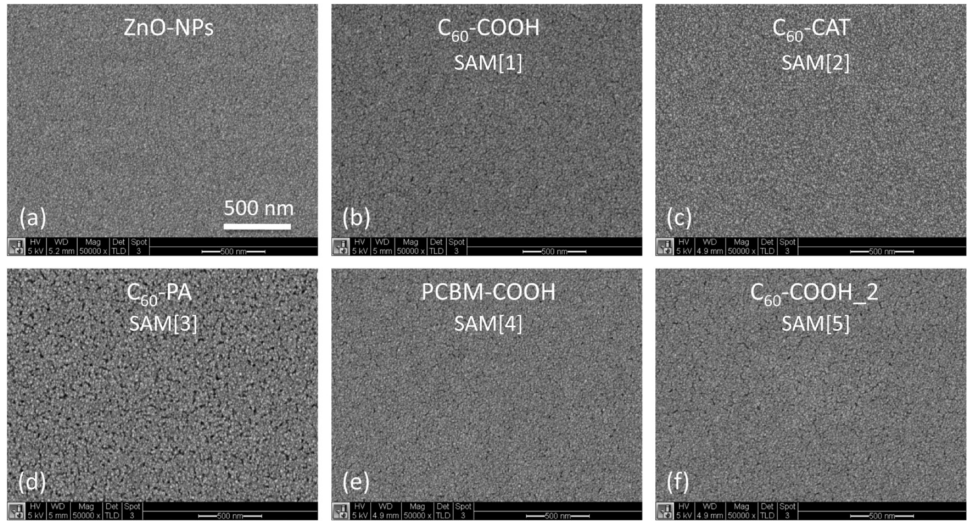

FIGURE 3. SEM image of (a) bare ZnO-NPs, 240 min assembly of (b) C_{60}-COOH SAM, (c) C_{60}-CAT SAM, (d) C_{60}-PA SAM, (e) PCBM-COOH SAM, and (f) C_{60}-COOH_2 SAM on ZnO-NPs. The C_{60}-PA SAM-processed film shows severe etching and degradation of the ZnO-NPs surface. Images were acquired at a magnification of 50 000×.

time alters the surface, thus explaining the reason for the lower contact angles at these times. The carboxylic acid based C_{60}-SAMs also show some slight signs of etching as can be seen by the initial stage of void formation in the SEM images, but the severity is much less than the phosphonic acid C_{60}-SAM. Interestingly, the weakly acidic catechol-based C_{60}-SAMs show a very similar surface profile to that of the unmodified ZnO-NPs, indicating minimum degradation due to etching even when assembled for long periods of time.

C_{60}-SAM-Modified Heterojunction Solar Cells. After characterizing the unmodified and C_{60}-SAM-modified ZnO-NP surfaces, we fabricated and compared inverted polymer-based solar cells using three SAM processing conditions (spin-coated, 10 min immersion, and 240 min immersion). These three different conditions are chosen on the basis of the simplicity for utilizing a spin-coating method to form the SAM, the optimized solution immersion method to form the SAM, and the over exposure of the acidic SAM solution to the ZnO-NP substrate. To understand the effect of the different C_{60}-based SAMs at the ZnO-NP interface, heterojunction solar cells consisting of the layers ITO/ZnO-NP/C_{60}-SAM/P3HT/PEDOT:PSS/Ag were fabricated. Because exciton dissociation occurs only at the ZnO-NP/C_{60}-SAM/P3HT interface, the effect of the different anchoring groups, linkage, and functionalization of the C_{60}-SAMs on the solar cell device parameters can be independently studied. Table 1 summarizes the average device performances of the unmodified and C_{60}-SAM modified heterojunction devices fabricated from the three different SAM processing conditions. The performance of the heterojunction devices fabricated without the SAM has an average open circuit voltage (V_{oc}) of 0.66 V, a short circuit current (J_{sc}) of 1.28 mA/cm^2, a fill factor (FF) of 37.8%, and power conversion efficiency (PCE) of 0.32%. It is well-known that the difference in the polymer highest occupied molecular orbital (HOMO) and the n-type semiconductor conduction band (CB) determines the upper limit of the V_{oc} and based on the P3HT and ZnO system these values can be high. The low fill factor in these devices is due to the poor interfaces between the hydroxy-

Table 1. Average Device Performance of Inverted ZnO NP/C_{60}-SAM/P3HT Heterojunction Solar Cells Fabricated onGlass/ITO Substrates. C_{60}-SAMs were Processed onto the Layer of ZnO-NPs by Either a Solution Spincoating Method or Solution Immersion Technique for 10 and 240 min; Average was Obtained from Multiple Device Tests

SAM	assembly time (min)	V_{oc} (V)	J_{sc} (mA/cm^2)	FF (%)	PCE (%)	contact angle (deg)
none	N/A	0.66	1.28	37.8	0.32	30.5
SAM[1]	spin-coat	0.56	2.36	52.4	0.69	67.8
	10	0.57	2.31	52.3	0.68	66.8
	240	0.51	2.10	54.6	0.58	61.9
SAM[2]	spin-coat	0.48	2.23	51.9	0.56	54.2
	10	0.47	2.12	52.8	0.52	59.4
	240	0.40	2.12	52.0	0.44	56.4
SAM[3]	spin-coat	0.56	1.11	39.6	0.25	47.8
	10	0.55	1.62	47.1	0.42	56.5
	240					47.0
SAM[4]	spin-coat	0.63	2.49	45.6	0.72	55.1
	10	0.64	2.21	50.3	0.71	62.2
	240	0.63	2.28	46.2	0.67	64.2
SAM[5]	spin-coat	0.52	2.36	54.8	0.68	73.3
	10	0.49	2.36	54.6	0.62	67.3
	240	0.48	2.25	54.1	0.59	71.7

lated surface of ZnO-NPs and P3HT which causes carrier losses due to charge recombination.

When modified with the C_{60}-SAMs, the heterojunction devices show an overall improvement in fill factor, photocurrent, and PCE depending on the SAM and the processing condition. Figure 4 shows the plots comparing the effect of the different C_{60}-based SAMs and its processing condition on the V_{oc}, J_{sc}, FF, and PCE of heterojunction devices. Figure 4a shows the plot of the variation of the V_{oc} with the different processing condition as well as the different C_{60}-based SAM. When modified with the carboxylic acid anchoring group (SAM[1]), the V_{oc} decreases from 0.66 to 0.56 V after 10 min of assembly and further decreases to 0.51 V after 240 min of assembly.

The lower V_{oc} after modification is attributed to the interfacial dipole formed from the carboxylic acid anchoring to surface of the ZnO-NPs (10). With the catechol anchoring group (SAM[2]), the V_{oc} decreases to 0.48 V after assembly for 10 min and 0.40 V after 240 min. The even lower V_{oc} after SAM[2] modification compared to that of SAM[1] can be attributed to the formation of a strong interface dipole because of catechol forming bidentate bonding, which leads to an intramolecular ligand to metal charge transfer transisition (28−33). For the phosphonic acid anchoring group (SAM[3]), the V_{oc} is 0.55 V after assembly for 10 min. However, after 240 min of assembly with SAM[3], the device did not behave as a photodiode and did not generate any solar cell performance. This is attributed to the degradation and etching of the ZnO-NPs layer because of the acidic nature of the phosphonic acid SAM as shown from the AFM and SEM images.

For SAM[4], the V_{oc} remains high and relatively constant at around 0.63 V under all three SAM processing conditions even though it has a carboxylic acid anchoring group. The high V_{oc} compared to that of the other C_{60}-based SAMs is due to the bifunctionalization of the C_{60} leading to a lower-energy LUMO, which helps to offset the effect from the interfacial dipole caused by the binding at the surface. It has been found that bifunctionalization of C_{60} can lead to a LUMO energy level shift of 0.1 eV and has led to increases in V_{oc} of ∼0.15 V in BHJ solar cells (34). Changing the linkage to the C_{60} molecule (SAM[5]) shows a slight decrease in V_{oc} compared to SAM[1]. Modification with SAM[5] leads to a V_{oc} of 0.49 and 0.48 V after assembling for 10 and 240 min, respectively. The different anchoring group, linkage, and functionalization of the SAM can lead to large variations in V_{oc} after modification. It is important to understand how to control the V_{oc} because this parameter affects the overall solar cell efficiency.

Another important parameter affecting the solar cell efficiency is the J_{sc} and the effects of the different C_{60}-based SAMs on this parameter are plotted in Figure 4b. In general, the photocurrent when modified with the C_{60}-based SAM shows an overall 2-fold enhancement from ∼1.28 mA/cm^2 to ∼2.1−2.5 mA/cm^2 compared to devices without any C_{60} modification indicating the improved photoinduced charge transfer properties at the ZnO-NP and P3HT interface. This improved photoinduced charge transfer property from P3HT to C_{60} is due to the excellent electron-accepting ability of the C_{60} molecule (35).

The variations in photocurrent from the different SAM processing conditions are minimal except for the C_{60} phosphonic acid anchoring SAM (SAM[3]). Under the optimized assembly time for SAM[3], the J_{sc} was around 1.62 mA/cm^2 and showed no photovoltaic effect when processed for 240 min. The lower J_{sc} compared to that of the other C_{60}-based SAMs may be attributed to slower electron-transfer process of the phosphonic acid anchoring group (36, 37).

The improvement from the C_{60}-based SAMs is also observed by the improved fill factors (Figure 4c). Reducing the hydroxyl groups on the ZnO surface by forming bonds with C_{60}-based SAMs reduces the resistance and recombination losses leading to improvement of fill factors from ∼37.1% to ∼45−55%. Similar to the J_{sc}, the fill factor does not vary much with the SAM processing condition for all the C_{60}-based SAMs apart from SAM[3] because of the etching of the ZnO-NP surface. The PCE of the heterojunction devices improves 2-fold (∼0.62 − 0.72%) with all the carboxylic-acid-based C_{60}-SAMs under the spin-coating and optimized 10 min processing conditions (Figure 4d). Immersion of SAM[1] and SAM[5] at longer times leads to a reduction in the PCE because of the lower V_{oc} under this processing condition. whereas for SAM[4], the PCE remained similar to those processed by spin-coating and by immersion for 10 min because of the unchanged V_{oc} with longer immersion times. For the catechol-based SAM, the PCE is only improved to ∼0.44−0.56% because of the much lower V_{oc} compared to that of the carboxylic-acid-based SAMs. For the phosphonic-acid-based SAM, the PCE under the optimized SAM assembly process gives an efficiency of 0.42%. Assembling for shorter

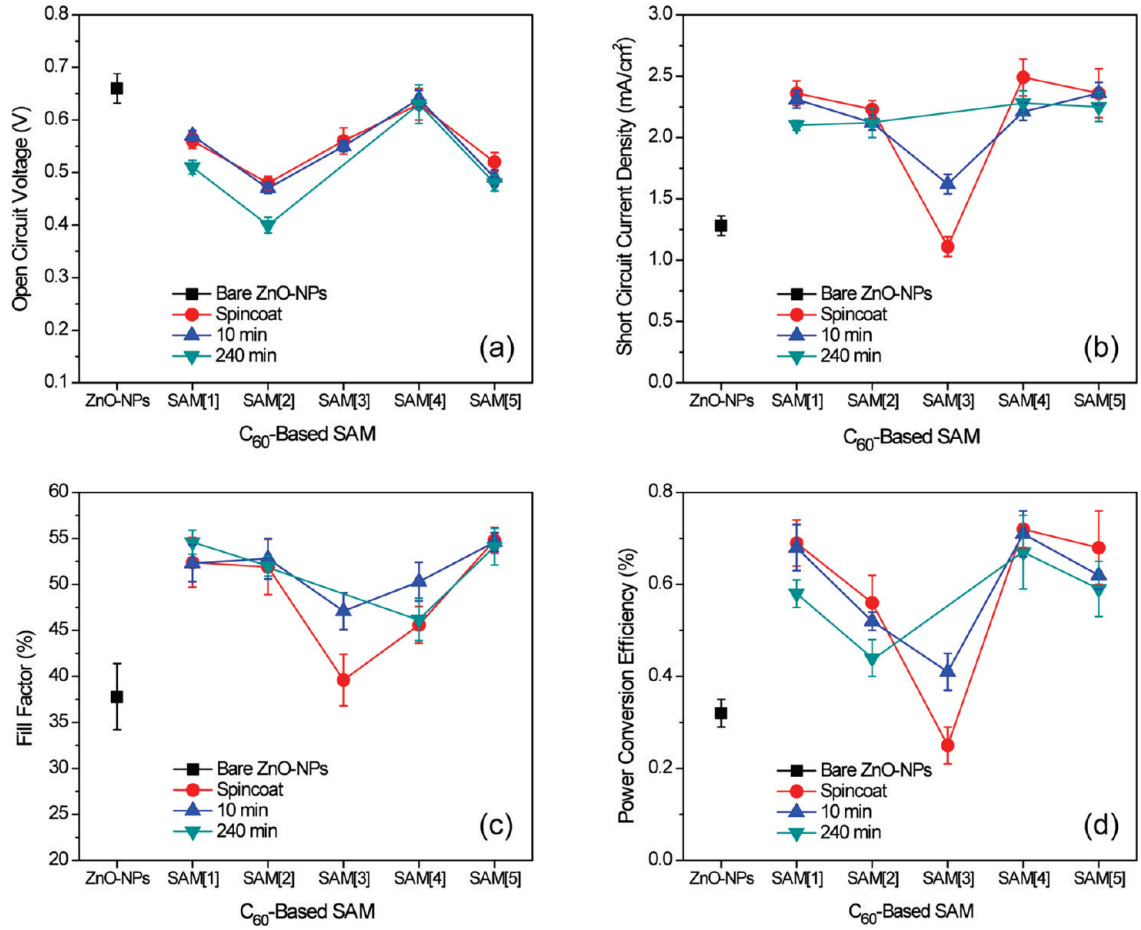

FIGURE 4. Plots comparing the effect of five different C_{60}-based SAMs on the (a) V_{oc}, (b) J_{sc}, (c) FF, and (d) PCE of heterojunction devices under three SAM processing conditions (spin-coating, 10 min immersion assembly, and 240 min immersion assembly) to heterojunction devices without any SAM modification.

time leads to lower solar cell efficiency and assembling for longer time etches the ZnO layer leading to devices that show no solar cell efficiency. The different anchoring groups for the SAM modification on ZnO leads to variations in V_{oc} caused by the differences in interface dipole upon binding to the metal oxide surface in heterojunction devices. The V_{oc} is affected not only by the anchoring group in these C_{60}-SAMs but also by the linkage and functionalization of the C_{60} that can further reduce the V_{oc} (SAM[5]) or increase the V_{oc} (SAM[4]). In addition, because of the differences in affinity and acidity of each of the anchoring groups to ZnO, the processing conditions can affect the formation of the SAM and affect the quality of the ZnO layer leading to improvement in PCE to over 0.7% in heterojunction solar cells. In some cases, the acidity of the SAM can etch the ZnO layer, leading to solar cells that do not function.

C_{60}-SAM Modified Bulk-Heterojunction Solar Cells. Inverted polymer-based bulk-heterojunction solar cells are fabricated with and without the C_{60}-based SAM at the ZnO-NP interface using the same three SAM processing conditions as those used for the heterojunction devices. The average performance of these solar cells are summarized in Table 2 and the effect of the SAM and SAM processing condition on the four device parameters are plotted in Figure 5. For the BHJ device without any SAM modification, the

Table 2. Average Device Performance of Inverted ZnO NP/C_{60}-SAM/P3HT:PCBM Bulk Heterojunction Solar Cells Fabricated on Glass/ITO Substrates[a]

SAM	assembly time (min)	V_{oc} (V)	J_{sc} (mA/cm^2)	FF (%)	PCE (%)	contact angle (deg)
None	N/A	0.60	10.07	57.7	3.47	30.5
SAM[1]	spin-coat	0.62	11.17	64.1	4.40	67.8
	10	0.61	11.12	64.0	4.36	66.8
	240	0.61	11.18	62.4	4.27	61.9
SAM[2]	spin-coat	0.61	10.66	60.4	3.93	54.2
	10	0.61	10.86	62.4	4.13	59.4
	240	0.61	11.21	61.0	4.19	56.4
SAM[3]	spin-coat	0.60	10.81	52.9	3.43	47.8
	10	0.62	10.27	62.6	3.96	56.5
	240					47.0
SAM[4]	spin-coat	0.60	11.00	56.3	3.68	55.1
	10	0.62	10.85	63.6	4.24	62.2
	240	0.61	10.86	63.3	4.22	64.2
SAM[5]	spin-coat	0.61	11.00	63.4	4.26	73.3
	10	0.61	11.26	62.4	4.30	67.3
	240	0.61	11.29	62.7	4.32	71.7

[a] The C_{60}-SAMs were processed onto the layer of ZnO-NPs by either a solution spin-coating method or solution immersion technique for 10 and 240 min. Average was obtained from multiple device tests.

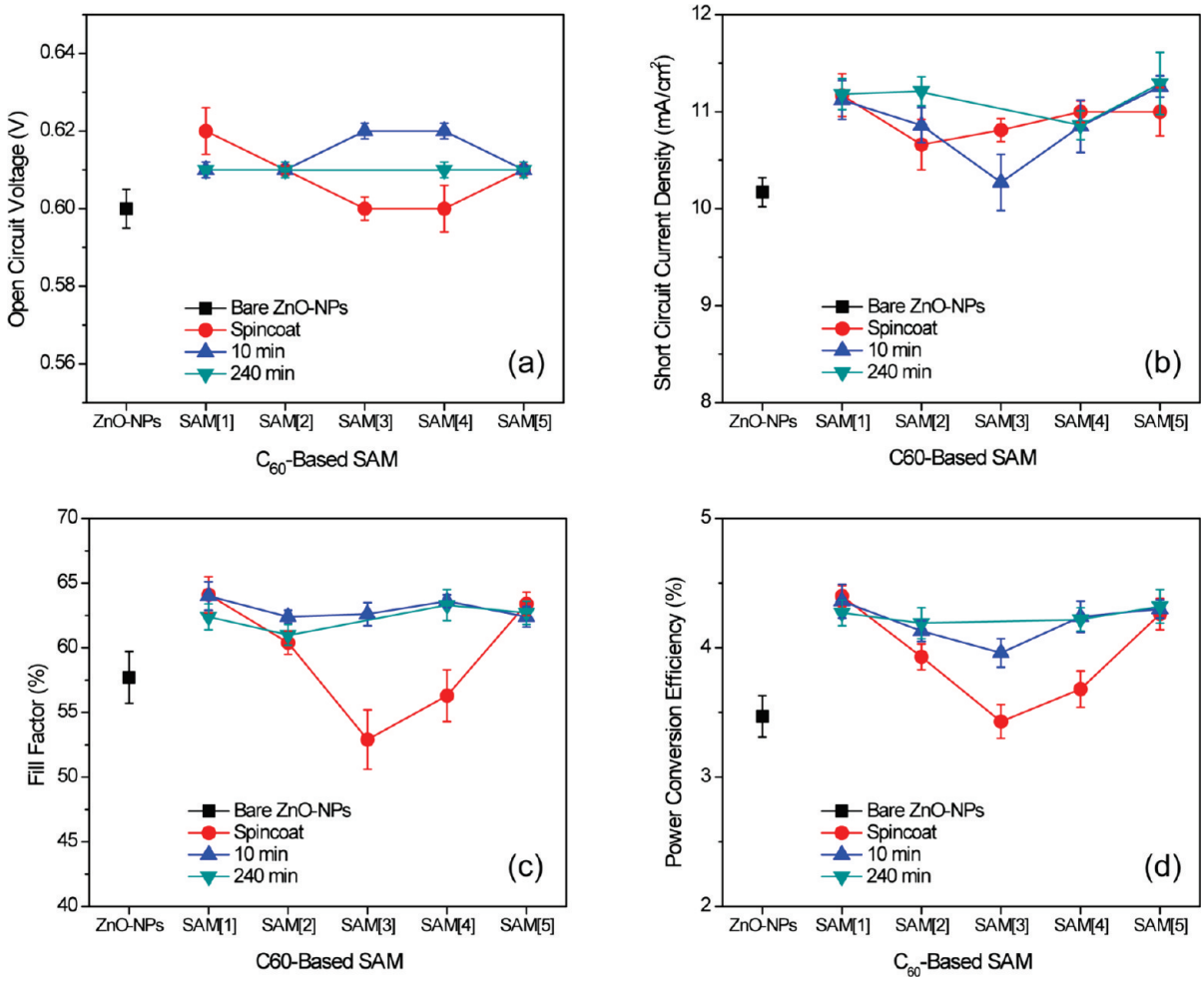

FIGURE 5. Plots comparing the effect of five different C_{60}-based SAMs on the (a) V_{oc}, (b) J_{sc}, (c) FF, and (d) PCE of bulk-heterojunction devices under three SAM processing conditions (spin-coating, 10 min immersion assembly, and 240 min immersion assembly) to bulk-heterojunction devices without any SAM modification.

average device parameter performance for $V_{oc} = 0.60$ V, $J_{sc} = 10.07$ mA/cm^2, FF = 57.7%, and PCE = 3.47%. Unlike the heterojunction devices, the variations in the V_{oc} in these devices are not significant, as shown in Figure 5a, which shows the V_{oc} for all the SAMs and SAM processing conditions to be around 0.60−0.62 V except for SAM[3] processed for 240 min, which again shows no photovoltaic effect due to the etching of ZnO. The main contribution for the V_{oc} in the BHJ is from the blend of the p-type P3HT and n-type PCBM materials because the number of interfaces is much greater than that from the ZnO and P3HT interfaces. Thus, the V_{oc} values of these BHJ solar cells with and without SAM modification are all very similar.

The photocurrent, however, shows a general 5−12% improvement over the unmodified inverted cells (Figure 5b), which is attributed to the additional C_{60}-SAM improving photoinduced charge transfer properties the from P3HT to the C_{60}-SAM/ZnO interface. As shown in the heterojunction devices without SAM modification, the photocurrents are relatively low due to the poor interfaces between the polymer and the ZnO layer. The addition of the C_{60}-SAM helps to minimize recombination losses at the interface because of the improved charge transfer from the polymer to the ZnO layer as can be seen by the improved photocurrent. Additionally, the fill factors of the devices are improved to over 60% when processed with the SAM (Figure 5c) showing that the C_{60} acts as a good electron selective layer and hole blocking layer to minimize recombination losses at the ZnO interface, which can also help to contribute to the higher photocurrent in these devices. The processing of the SAM seems to have a slight influence on the photocurrent showing that longer assembly have higher photocurrent than those processed by spin-coating. However, SAM[1] shows no major variation in photocurrent from the processing, indicating that the formation of the SAM by spin-coating is just as good as immersion of the sample for longer times. A noticeable change in photocurrent is observed with the catechol-based SAM (SAM[2]) when processed from spin-coating and immersion showing a increase in photocurrent when processed at longer times. Furthermore, the fill factors are the highest when the SAMs are process under the optimum 10 min solution immersion condition. The conversion efficiency of the C_{60}-SAM modified devices are improved by ∼6−28% compared to devices without SAM modification (Figure 5d).

The illuminated $J-V$ characteristics of the C_{60}-based SAMs assembled for 10 and 240 min are shown in Figure 6. The highest efficiencies were achieved by utilizing a SAM with

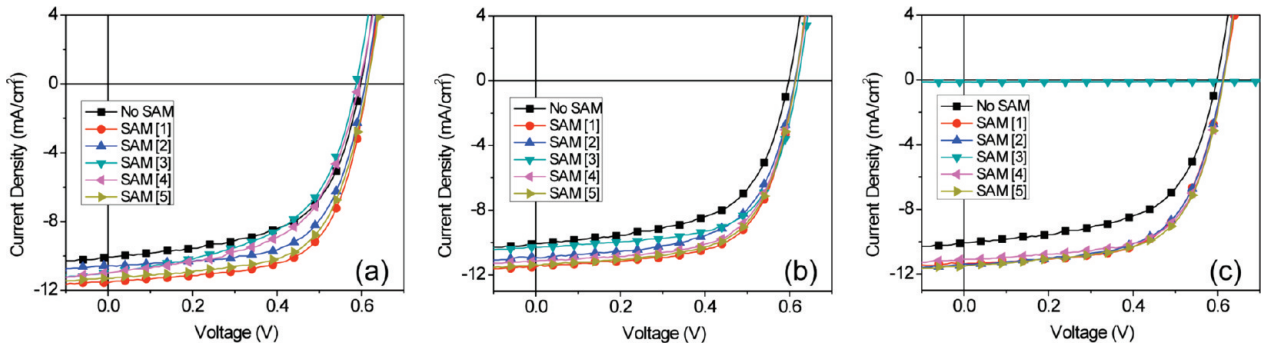

FIGURE 6. Plots comparing the $J-V$ characteristics of inverted bulk-heterojunction solar cells with C_{60}-SAM modification processed by (a) spin-coating from a 1 mM solution, (b) 10 min solution immersion, and (c) 240 min solution immersion to devices without modification.

the carboxylic acid anchoring group leading to average efficiencies of 4.4%. The carboxylic-acid-based SAMs all show efficiency improvements over 4.2% even under long-term assembly of the SAM, indicating the acidity of the carboxylic acid anchoring group may only slightly degrade the ZnO layer as shown by the SEM images. The least-acidic SAM (catechol) shows an increase in efficiency to 3.93% when the SAM is spin-coated, 4.13% when the SAM is assembled for 10 min, and 4.19% when the SAM is assembled for 240 min. The increase in efficiency with longer assembly time shows that the acidity of the anchoring group of the SAM does not degrade the ZnO layer, as indicated from the SEM images taken at 240 min of assembly. For the most-acidic SAM (phosphonic acid) in this series, the assembly for the optimized 10 min shows conversion efficiency of 3.96%; however, longer assembly causes etching of the ZnO layer, as seen by the SEM image, leading to cells that do not function.

CONCLUSIONS

In conclusion, altering the anchoring group, linkage, and bis-functionalization of the C_{60}-SAM affects the V_{oc} and FF of ZnO-NP/C_{60}-SAM/P3HT heterojunction devices because of the interface dipole formed from the different anchoring groups and the improved photoinduced charge transfer properties which reduce the losses from recombination, respectively. In general, the C_{60}-SAM modification leads to over a 2-fold improvement in efficiency (0.58−0.72%) for the carboxylic-acid-based C_{60}-SAMs, a slightly lower improvement (0.44−0.56%) for the catechol-based C_{60}-SAM because of the lower V_{oc}, and a slight improvement (0.42%) from the C_{60}-phosphonic acid based SAM. However, the effect of the C_{60}-SAMs on the V_{oc} are less significant in BHJ devices, because the interface controlling this parameter is primarily from the interface between the active donor and acceptor blend layer. The two parameters that contribute to the improvement of BHJ cells when modified with a C_{60}-SAM are the J_{sc} and FF because of the improvement in the interface between the ZnO-NPs and the P3HT/PCBM blend. The C_{60}-SAM helps to minimize charge recombination losses at the interface by removing charge trapping hydroxyl groups by binding to the ZnO surface as well as improves the photoinduced charge transfer properties. Under the optimized SAM assembly condition, the efficiency is improved from 3.47% (without modification) to ~4.4% (with the carboxylic acid C_{60}-SAMs), 4.19% (with the catechol C_{60}-SAM), and 3.96% (with the phosphonic acid C_{60}-SAM). Different processing conditions for forming the SAM are studied to optimize the SAM assembly process because the different affinities of the anchoring groups to the surface of ZnO. The C_{60}-SAMs are processed and formed onto the layer of ZnO nanoparticles by either a solution immersion technique or a solution spin-coating method. It is found that the C_{60}-SAMs with the carboxylic acid and catechol anchoring groups can be formed onto the surface of ZnO by a simple solution spin-coating process, whereas all three anchoring groups can be formed onto ZnO by a solution immersion technique. The optimum time for solution immersion is dependent on the anchoring group due their differences in binding affinity to ZnO. However, because of the differences in acidity of the anchoring groups, immersing the ZnO substrate for a long period of time into a solution containing the C_{60}-carboxylic acid SAMs leads to slight etching of the ZnO surface, which shows a slight decrease in device performance. When immersing in a C_{60}-phosphonic acid SAM solution, significant etching of the ZnO occurs leading to nonfunctional solar cells. When immersing in a C_{60}-catechol SAM solution, the etching of ZnO is insignificant, which leads to high efficiency solar cells even after immersion for longer times. Understanding the affect of the SAM anchoring group on ZnO is important for designing new interface modifiers to minimize losses caused by etching of the ZnO surface because of the acidity of the anchoring group as well as the interface dipoles formed from the binding to maximize the performance of inorganic/organic hybrid and dye-sensitized based solar cells.

Acknowledgment. This work was supported by the National Science Foundation's NSF-STC program under Project DMR-0120967, the DOE "Future Generation Photovoltaic Devices and Process" program under ProjectDE-FC36-08GO18024/A000, and the World Class University (WCU) program through the National Research Foundation of Korea under the Ministry of Education, Science, and Technology (R31-10035). A.K.Y.J. thanks the Boeing-Johnson Foundation for financial support. Authors would like to thank Prof Brian Flinn at the University of Washington for the use of their Ramé-Hart 100 Goniometer. Instrumentation for scanning electron microscopy was provided by the Nanotechnology

User Facility (NTUF), a member of the National Nanotechnolgoy Infrastructure (NNIN) supported by NSF.

Supporting Information Available: Differential scanning calorimetry of fullerene materials, contact angle and surface energy measurements for C_{60}-SAMs (PDF). This material is available free of charge via the Internet at http://pubs.acs.org.

REFERENCES AND NOTES

(1) Liang, Y.; Wu, Y.; Feng, D.; Tsai, S.-T.; Son, H.-J.; Li, G.; Yu, L. *J. Am. Chem. Soc.* **2009**, *131* (1), 57.
(2) Liang, Y.; Feng, D.; Wu, Y.; Tsai, S.-T.; Li, G.; Ray, C.; Yu, L. *J. Am. Chem. Soc.* **2009**, *131* (22), 7792.
(3) Park, S.-H.; Roy, A.; Beaupre, S.; Cho, S.; Coates, N.; Moon, J.-S.; Moses, D.; Leclerc, M.; Lee, K.; Heeger, A. J. *Nat. Photonics* **2009**, *3*, 297.
(4) de Jong, M. P.; van IJzendoorn, L. J.; de Voigt, M. J. A. *Appl. Phys. Lett.* **2000**, *77*, 2255.
(5) Hau, S. K.; Yip, H.-L.; Baek, N. S.; Zou, J.; O'Malley, K.; Jen, A. K.-Y. *Appl. Phys. Lett.* **2008**, *92*, 253301.
(6) Hau, S. K.; Yip, H.-L.; Leong, K.; Jen, A. K.-Y. *Org. Electron.* **2009**, *10*, 719.
(7) Takanezawa, K.; Tajima, K.; Hashimoto, K. *Appl. Phys. Lett.* **2008**, *93*, 063308.
(8) Huang, J. S.; Chou, C. Y.; Liu, M. Y.; Tsai, K. H.; Lin, W. H.; Lin, C. F. *Org. Electron.* **2009**, *10*, 1060.
(9) Chua, L. L.; Zaumseil, J.; Chang, J.-F.; Ou, E. C.-W.; Ho, P. K.-H.; Sirringhaus, H.; Friend, R. H. *Nature* **2005**, *434*, 194.
(10) Goh, C.; Scully, S. R.; McGehee, M. D. *J. Appl. Phys.* **2007**, *101*, 114503.
(11) Hau, S. K.; Yip, H.-L.; Acton, O.; Baek, N. S.; Ma, H.; Jen, A. K.-Y. *J. Mater. Chem.* **2009**, *18*, 5113.
(12) Bardecker, J.; Ma, H.; Kim, T.; Huang, F.; Liu, M. S.; Cheng, Y. J.; Ting, G.; Jen, A. K.-Y. *Adv. Funct. Mater.* **2008**, (24), 3964.
(13) Hsu, C.-W.; Wang, L.; Su, W.-F. *J. Colloid Interface Sci.* **2009**, *329*, 182.
(14) Ting, G. G.; Acton, O.; Ma, H.; Ka, J. W.; Jen, A. K.-Y. *Langmuir* **2009**, *25* (4), 2140.
(15) Yip, H.-L.; Hau, S. K.; Baek, N. S.; Jen, A. K.-Y. *Appl. Phys. Lett.* **2008**, *92*, 193313.
(16) Yip, H.-L.; Hau, S. K.; Baek, N. S.; Ma, H.; Jen, A. K.-Y. *Adv. Mater.* **2008**, *20* (12), 2376.
(17) Zakeeruddin, S. M.; Nazeeruddin, M. K.; Pechy, P.; Rotzinger, F. P.; Humphry-Baker, R.; Kalyanasundaram, K.; Gratzel, M. *Inorg. Chem.* **1997**, *36*, 5937.
(18) Montalti, M.; Wadhwa, S.; Kim, W. Y.; Kipp, R. A.; Schmehl, R. H. *Inorg. Chem.* **2000**, *39*, 76.
(19) Oregan, B.; Gratzel, M. *Nature* **1991**, *353*, 737.
(20) Chou, T. P.; Zhang, Q.; Cao, G. *J. Phys. Chem. C* **2007**, *111*, 18804.
(21) Borgias, B. A.; Cooper, S. R.; Koh, Y. B.; Raymond, K. N. *Inorg. Chem.* **1984**, *23* (8), 1009.
(22) Moser, J.; Punchihewa, S.; Infelta, P. P.; Graetzel, M. *Langmuir.* **1991**, *7* (12), 3012.
(23) Hau, S. K.; Yip, H.-L.; Ma, H.; Jen, A. K.-Y. *Appl. Phys. Lett.* **2008**, *93*, 233304.
(24) Beek, W. J. E.; Wienk, M. M.; Kemerink, M.; Yang, X.; Janssen, R. A. J. *J. Phys. Chem. B* **2005**, *109*, 9505.
(25) Cravino, A.; Schilinsky, P.; Brabec, C. J. *Adv. Funct. Mater.* **2007**, *17*, 3906.
(26) Kim, M.-S.; Kang, M.-G.; Guo, L. J.; Kim, J. *Appl. Phys. Lett.* **2008**, *92*, 133301.
(27) Backer, S. A.; Sivula, K.; Kavulak, D. F.; Frechet, J. M. J. *Chem. Mater.* **2007**, *19*, 2927.
(28) Ramakrishna, G.; Ghosh, H. N.; Singh, A. K.; Palit, D. K.; Mittal, J. P. *J. Phys. Chem. B.* **2001**, *105*, 12786.
(29) Rodriguez, R.; Blesa, M. A.; Regazzoni, A. E. *J. Colloid Interface Sci.* **1996**, *177*, 122.
(30) Tae, E. L.; Lee, S. H.; Lee, J. K.; Yoo, S. S.; Kang, E. J.; Yoon, K. B. *J. Phys. Chem. B* **2005**, *109*, 22513.
(31) Kar, P.; Verma, S.; Das, A.; Ghosh, H. N. *J. Phys. Chem. C* **2009**, *113*, 7970.
(32) Marczak, R.; Werner, F.; Gnichwitz, J.-F.; Hirsch, A.; Guldi, D. M.; Peukert, W. *J. Phys. Chem. C* **2009**, *119*, 4669.
(33) Persson, P.; Bergstrom, R.; Lunell, S. *J. Phys. Chem. B* **2000**, *114*, 10348.
(34) Lenes, M.; Wetzelaer, G.-J. A. H.; Kooistra, F. B.; Veenstra, S. C.; Hummelen, J. C.; Blom, P. W. M. *Adv. Mater.* **2008**, *20*, 2116.
(35) Sariciftci, N. S.; Smilowitz, L.; Heeger, A. J.; Wudl, F. *Science* **1992**, *258*, 1474.
(36) Ernstorfer, R.; Gundlach, L.; Felber, S.; Storck, W.; Eichberger, R.; Willig, F. *J. Phys. Chem. B* **2006**, *110*, 25383.
(37) Li, J.; Nilsing, M.; Kondov, I.; Wang, H.; Persson, P.; Lunell, S.; Thoss, M. *J. Phys. Chem. C* **2008**, *112*, 12326.

AM100238E